Close-Coupling Guided Lenses for Gravity Triggered Pattern-Reconfigurable Antennas for Aerial Vehicles and Communication Systems

Siyu Li, *Student Member*, *IEEE*, Benito Sanz Izquierdo, *Member*, *IEEE*, Steven Gao, *Fellow, IEEE,* John Batchelor, *Senior Member*, *IEEE*, Zhijiao Chen, *Member*, *IEEE.*

***Abstract*— This paper introduces a novel close-coupling guided lens technique for gravity-triggered pattern-reconfigurable antennas for aerial vehicles and communication systems. The proposed technique utilizes purposefully designed curved containers where a lens can freely slide with gravity, serving as a versatile add-on for existing aerial devices. In a basic configuration with a cylindrical container and a centered half-wavelength dipole antenna, directivity increases by 3.1 dB, enabling 360° beam steering. In a more application-based set up using dielectric resonator antennas (DRAs) with semi-cylindrical/ semi-spherical lenses 1D/ 2D beam steering is achieved, effectively covering half-space areas. A continuous beam steering of ±35° is demonstrated for these applications. Both solid and liquid lenses have been employed flexibly, offering a broader range of options in practical applications, and extending the viability of the proposed concept. Furthermore, only a small volume of material (< 7 cm^3) is needed for the lens. A good agreement between the simulated and measured results for both liquid and solid lenses has been observed, proving the feasibility of the idea. This study provides a potential low cost, energy efficient, light weight solution for inclined static platforms such as aerial vehicles, communication balloons, or simply in vehicular scenarios involving anticipated tilts or rotations.**

***Index Terms*—pattern reconfiguration, ionic liquid, lens, aerial vehicle, vehicular communication**

I. Introduction

DUE to the ongoing rapid growth of the Internet-of-Things (IoT), fifth-generation (5G) and incoming sixth-generation (6G) communication systems in aerial vehicles, the demand for antennas with multifunctional capabilities, reconfigurability and compact space has significantly increased [1-5]. Reconfigurable antennas offer a promising solution to address this requirement. These antennas can dynamically control characteristics such as radiation pattern, resonant frequency, or polarization using external controlling circuits or systems that can produce a variable beam.

Pattern-reconfigurable antennas are suitable candidates for many vehicular applications such as dynamic beam-switching, direction-finding, null scanning and interference-avoiding [6]. They could provide several advantages, such as better spatial reuse, suppressing multipath interference, reduction of interference, and larger space coverages. They are perfectly suitable for applications that require dynamically tilting platforms such as aircraft, unmanned aerial vehicle (UAV), communication balloons and other aerial vehicles [7, 8] as illustrated in Fig. 1. In these applications, maintaining constant communication with a base station is crucial, regardless of the vehicle's platform angle. Therefore, the antenna must be able to adjust its beam direction in response to the orientation.

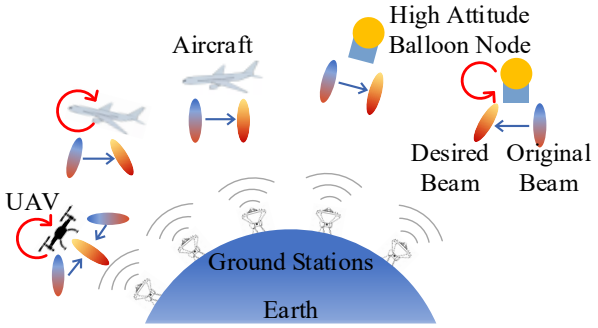

Fig. 1. Potential application scenario for the pattern-reconfigurable antennas in aircraft, unmanned aerial vehicle (UAV), high altitude balloons and other aerial vehicles and communication systems.

Recent advancements in achieving pattern reconfigurable antennas for vehicular communication systems have been documented [9-16]. Many of these initiatives utilize PIN diodes to switch between different states to control the radiated beam direction. This follows conventional reconfiguration methods, where commonly used analog phase shifters like PIN diodes [17], MEMS varactors [18], or other tunable components [19] are typically employed. While PIN diodes boast a low switching time, their high insertion loss at higher frequencies limits their applications. MEMS varactors exhibit lower loss and a high Q-value but might have limitations in power handling capability. Furthermore, no matter how compact each component is, as the total number of components in the system increases, the overall control circuitry becomes excessively large, leading to high power consumption. This limitation significantly hampers the practical applicability of the system.

Recently, beam steering antennas based on gravity have been documented [20, 21]. A beam steering coaxial-feed monopole antenna based on a separate reflect ground structure is proposed [20]. However, the structure is only capable of beam steering in one direction, with the rotation relying solely on a single coaxial cable. A beam steering DRA is proposed, wherein a ball lens is suspended alongside it using a string [21]. This setup provides a passive method for adjusting its radiation pattern through the influence of gravity on the ball lenses. Nevertheless, the ball lens is relatively heavy and large,

Siyu Li, Benito Sanz-Izquierdo, and John Batchelor are with the School of Engineering, University of Kent, Canterbury, CT2 7NZ, UK. (email: sl744@kent.ac.uk). Steven Gao is with the Department of Electronic Engineering, Chinese University of Hong Kong, Hong Kong, 518057, China. (email: scgao@ee.cuhk.edu.hk). Zhijiao Chen is with the Department of Electronic Engineering, Beijing University of Posts and Telecommunications, Beijing, 100876, China, (email: z.chen@bupt.edu.cn).

resulting in a bulky system overall. Additionally, relying solely on a string as the connection between the DRA and ball lens compromises the system's robustness and stability, especially in the face of turbulence and other practical scenarios. Besides, most of gravity-based pattern reconfigurable solutions mentioned above are limited to specific and predesigned antennas, limiting their applicability in existing aerial vehicles and communication systems.

This work overcomes the aforementioned challenges by introducing the concept of close-coupling guided lenses for gravity-triggered pattern-reconfigurable antennas. Employing curved containers, these lenses can freely slide to facilitate beam steering. As the loaded lens moves to a specific angle due to gravity, the primary beam emitted from the radiator adjusts its direction accordingly. This close-coupling guided lens technique is an add-on solution suitable for most types of antennas. When using a dipole antenna on a cylindrical container, 360° beam steering is achieved. To demonstrate the feasibility in more practical applications, solutions have been developed for 1D and 2D beam steering on DRAs. In the 1D configuration, the main radiated beam can be scanned along a single axis, while the 2D configuration achieves dual-axis scanning. Significantly, the 2D setup allows for a half-space beam steering range. A maximum ±35° of beam steering angle could be achieved when the rotation angle of lens θ reaches ±45°, where a gain deviation less than 1.5 dB is observed along with the steered beams. Both solid and liquid lenses were fabricated and tested. A minimal volume of material (< 7 cm^3) was required compared to alternative designs [22-24], offering a more versatile and cost-effective solution. This novel approach enables the steering of the radiated beam in applications where a platform tilt is anticipated. It holds relevance in civil aircraft, unmanned aerial vehicles (UAVs), high-altitude balloons, or in static platforms such as antennas within inclined structures in building communication systems.

The remaining of this paper is arranged as follows. The initial concept and its application to DRA-based reconfigurable antenna structures, along with simulation results and parametric analysis, are presented in Section II. Building upon these simulated results, the fabrication for the radiating DRA elements and solid lenses, the setup and results for measurements are presented in Section III. Finally, discussions and conclusions are given in Section IV and V, respectively.

II. Close-Coupling Guided Lenses Concept and Its Potential Applications in Practical Scenarios

A. Close-Coupling Guided Lens Concept

The close-coupling guided lens concept is depicted in Fig. 2 (a), comprising a radiator, a close-coupling guided lens acting as a director, and a cylindrical container housing the lens. The radiator can be of any type (e.g., dipole, patch, DRA), and similarly, the lens can be chosen flexibly, provided it can freely slide on a curved container. The director initially guides the radiated beam from the radiator in a specific direction. As the director moves freely along the container - driven by external forces such as gravity or mechanical actuation - the orientation of the beam dynamically follows this movement. This mechanism enables effective beam steering performance. In

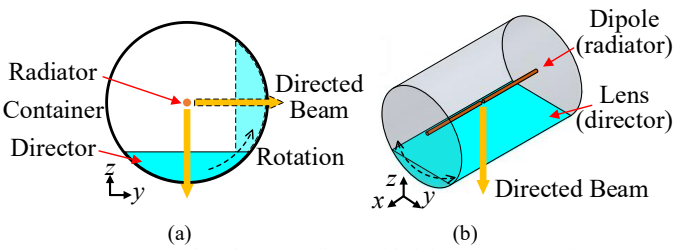

Fig. 2. Concept of the close-coupling guided lens. (a) general structure consisted of a radiator, a director, and a container. (b) example of concept including a dipole as radiator, liquid/ solid lens as director and a container.

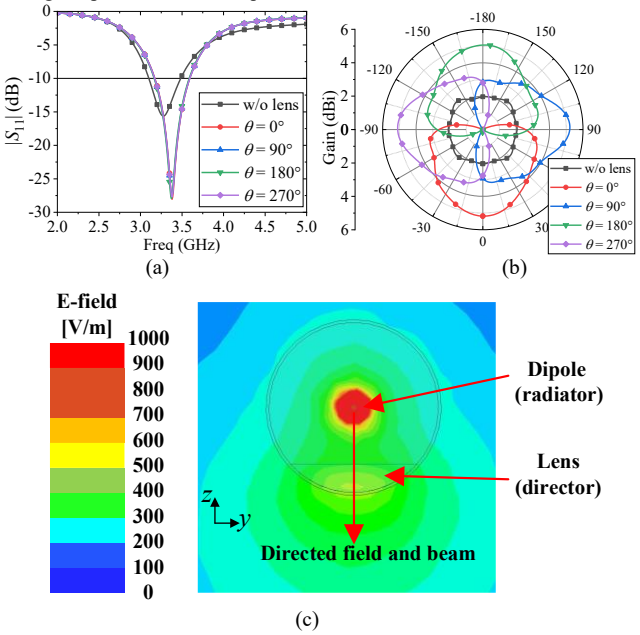

Fig. 3. *S*-parameters and radiation pattern of the dipole with and without the close-coupling guided lens in different rotation angles (θ). (a) *S*-parameters. (b) radiation patterns. (c) Diagram of coupling and director effect from the liquid/ solid lens on E-field.

this initial illustration, a half-wavelength dipole antenna, 40 mm in total length, is used as the main radiator for simplicity and conceptual demonstration, as shown in Fig. 2 (b). The cylindrical container has a diameter of 30 mm and a length of 45 mm, with the lens's height from the cylinder's edge set at 5 mm, resulting in a total volume of 3.48 cm^3.

The permittivity of the lens must be carefully chosen to balance the close-coupling lens effect and practical cost considerations. In this case, $\varepsilon_r = 9$ and $\tan\delta = 0.2$ are employed, which is consistent to the material used in subsequent sections. The lens is designed to convert the omnidirectional beam of the dipole antenna into a directional one, enhancing gain and steering the beam as it rotates around the centerline of the dipole. The structure was optimized for maximum gain and beam steering performance.

The *S*-parameters and radiation patterns at different lens rotation angles are depicted in Fig. 3 (a) and (b), with the radiation pattern presented at 3.3 GHz. The reflection coefficient improves when loading the lens. The gain is enhanced from 2.1 to 5.2 dBi, and a distinct directional beam is evident. Besides, a 360° beam steering angle can be achieved through lens rotation, providing full-space beam steering coverage. The electric field in Fig. 3 (c) demonstrates the coupling and director effects, explaining the gain enhancement

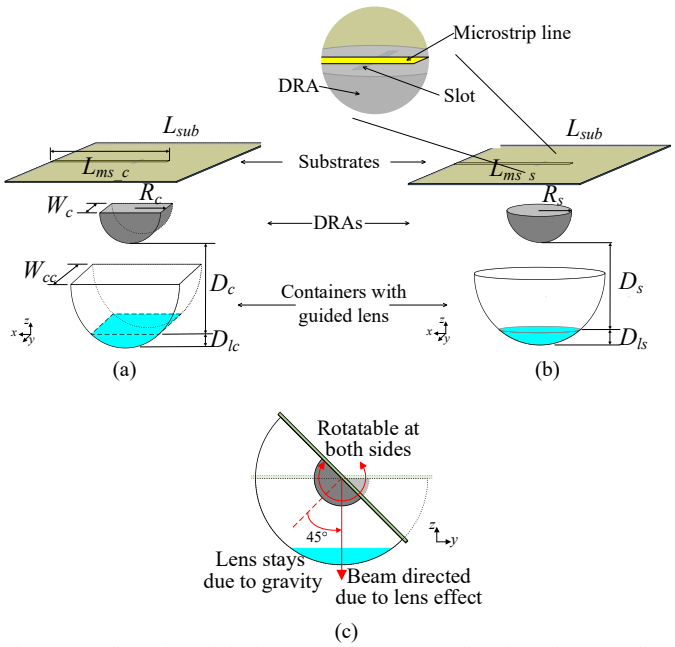

Fig. 4. Configuration of the beam steering antennas based on close-coupling guided lens. (a) 1D beam steering DRA with semi-cylindrical container. (b) 2D beam steering DRA with semi-spherical container. (c) diagram of proposed structure when rotated at 45°.

TABLE I
KEY DIMENSION PARAMETERS OF PROPOSED BEAM STEERING ANTENNA

Parameters	L_{sub}	L_{ms_c}	R_c	W_c
Value (mm)	100	54.7	15	20
Parameters	D_c	W_{cc}	D_{lc}	L_{ms_s}
Value (mm)	4	30	8	56.2
Parameters	R_s	D_s	D_{ls}	
Value (mm)	15	7	8	

and beam steering performance in Fig. 3 (b) and confirming the feasibility of the proposed concept.

B. Application of Close-Coupling Guided Lenses to DRAs for Aerial Vehicles and Communication Systems

The close-coupling guided lens concept is applicable to antennas on platforms requiring tilt such as those in aerial vehicle applications illustrated in Fig.1. Ideally, the antenna should provide full coverage of the lower half-space as the platform changes its angle. However, due to flying characteristics and the distance between the air vehicle and the ground station, about ±35° 2D beam steering angle is sufficient.

To demonstrate the feasibility of the proposed concept, two close-coupling guided lens DRA solutions were developed for this application, namely the 1D and 2D configurations, as depicted in Fig. 4. The 1D configuration enables beam steering in a single direction, while the 2D configuration allows free beam steering in any direction beneath the antenna. They consist of three main parts: a feeding network, a dielectric resonator antenna (DRA), and a container housing a lens that steer the beam through gravitational rotation. The lens represented blue in this illustration.

The DRAs are fed by slot coupled microstrip lines with impedance of 50 Ω. The base substrates are the Rogers RO4003C (ε_r = 3.66, tanδ = 0.004, and thickness = 0.508 mm). Both DRAs are designed to produce a single linearly-polarized

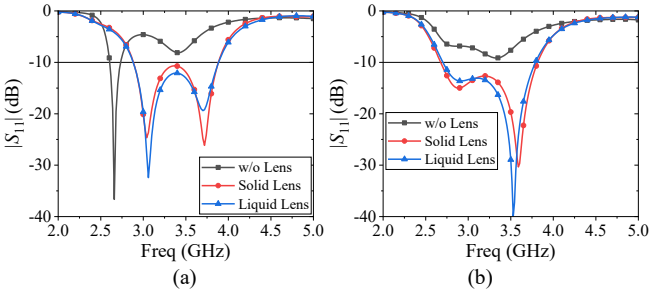

Fig. 5. *S*-parameters of the proposed antennas without and with different types of lenses. (a) 1D beam steering semi-cylindrical DRA. (b) 2D beam steering semi-spherical DRA.

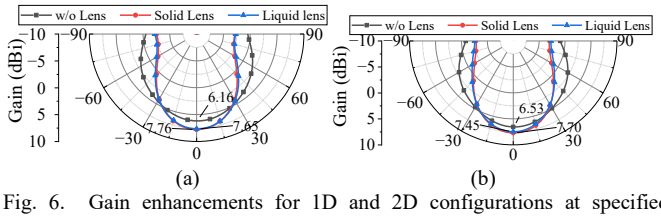

Fig. 6. Gain enhancements for 1D and 2D configurations at specified frequencies. (a) 1.6 dB enhancement for 1D beam steering semi-cylindrical DRA at 3.2 GHz. (b) 1.2 dB enhancement for 2D beam steering semi-spherical DRA at 3.6 GHz.

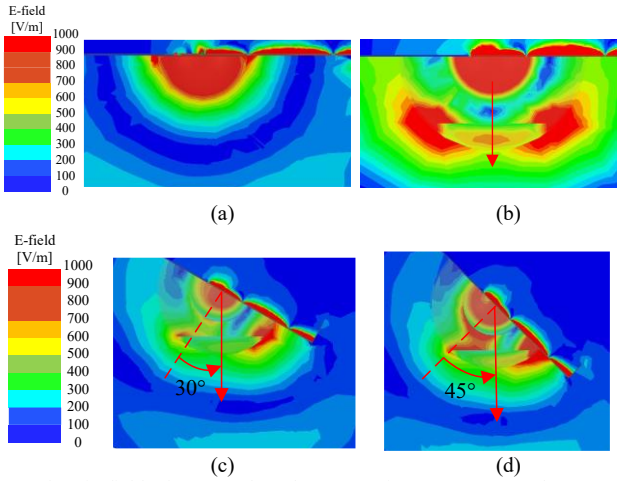

Fig. 7. Electric field of proposed 2D beam steering DRA at yoz plane at 3.6 GHz when (a) without the lens; and with the lens at rotation angle θ = (b) 0°, (c) 30°, (d) 45°.

pencil beam radiation pattern. The detailed dimensions are listed in Table I. The physical dimensions of both the DRA and the associated dielectric lenses can be significantly reduced by utilizing materials with higher relative permittivity. As demonstrated in [25], employing a typical ceramic material with a relative permittivity (ε_r) in the range of 30 – 50 can reduce the DRA radius by approximately 1/2, thereby decreasing its volume by 1/4. Moreover, the dimensions of the dielectric director can also be minimized through the use of high-permittivity materials, without compromising its electromagnetic performance. By loading the containers with the lenses, two variants of beam steering antennas can be achieved. The lens in semi-cylindrical container (Fig. 4. (a)) could rotate along the y-axis thus achieving 1D beam steering. Conversely, in the case of the semi-spherical container, the lens has the capacity to rotate along both x- and y-axis, resulting in 2D beam steering capability in the lower half space below xoy plane.

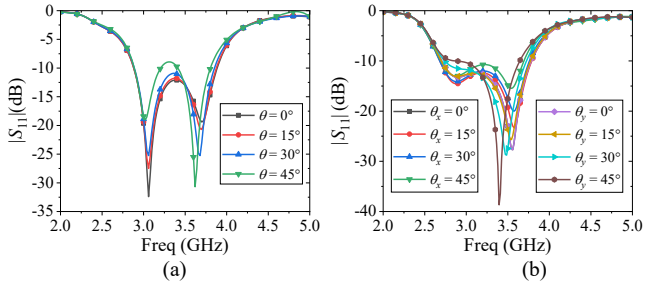

Fig. 8. Simulated S_{11} for various rotation angles. (a) 1D beam steering semi-cylindrical DRA. (b) 2D beam steering semi-spherical DRA.

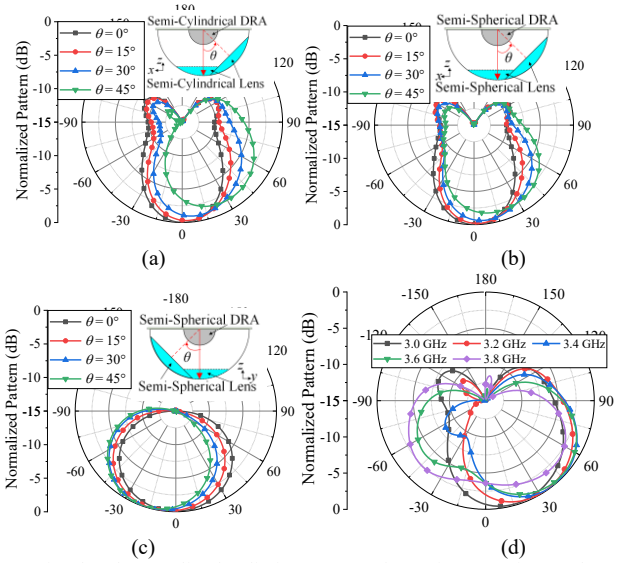

Fig. 9. Simulated normalized radiation patterns for various rotation angles. (a) 1D beam steering semi-cylindrical DRA. (b) 2D beam steering semi-spherical DRA with x-scanning. (c) 2D beam steering semi-spherical DRA with y-scanning. (d) beam steering performance at different frequencies when $\theta = 45°$ for 1D beam steering semi-cylindrical DRA.

The guided lenses could be in either solid or liquid form, provided they have similar electrical characteristics and the ability to move freely along the surface of the container. For simulation purposes, the lens was modeled as a dielectric block resembling a partial cylinder or a spherical cap. The electrical characteristics of PREPERM® ABS1000 with dielectric constant (ε_r) of 10 ± 0.35 and loss tangent (tan δ) of 0.003 was used for the solid lens [26], while choline L-alanine with ε_r ranging from 8 - 12 and tan δ ranging from 0.02 to 0.1, between 1 – 5 GHz [27] was chose for the liquid lens.

The 1D and 2D beam steering DRAs with and without the lens were simulated to analyze the impact of the lens loading. As can be seen from Fig. 5, the reflection coefficient improves, and the working band is broadened when the lenses are loaded. As shown in Fig. 6, the broadside gains are enhanced by 1.6 dB and 1.2 dB for 1D and 2D cases, respectively. This proves the directional effect of the lenses. All gain values correspond to well-matched radiator configurations to eliminate potential effects from impedance mismatch. Matching was achieved by adjusting the dimensions of the microstrip feed lines and coupling slots, which had negligible impact on the radiation characteristics of the DRAs.

Due to the similar performance for the solid and liquid lenses observed from Fig. 5 and 6, the subsequent discussions will primarily focus on the liquid lens. This choice was made

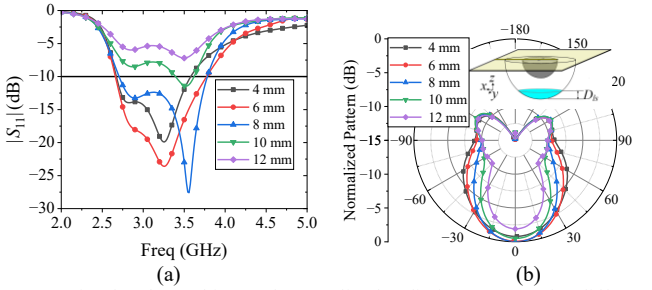

Fig. 10. Simulated matching and normalized radiation patterns for different volume (Dls). of the lens. (a) S_{11}. (b) normalized radiation pattern at 3.6 GHz.

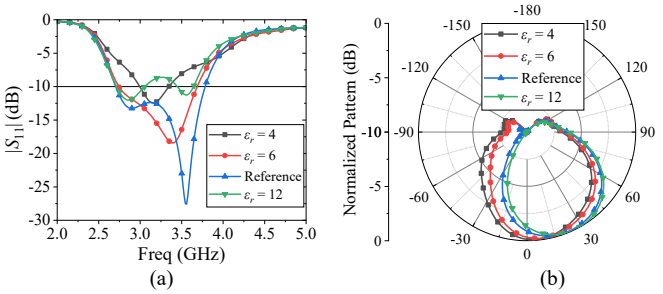

Fig. 11. Simulated matching and normalized radiation patterns for different permittivity (ε_r) of the lens. (a) S_{11}. (b) normalized radiation pattern for $\theta = 45°$ at 3.6 GHz.

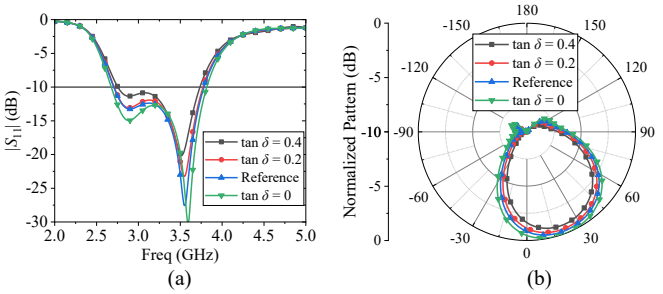

Fig. 12. Simulated matching and normalized radiation patterns for different loss tangent (tanδ) of the lens. (a) S_{11}. (b) normalized radiation pattern for $\theta = 45°$ at 3.6 GHz.

because the liquid lens exhibits greater complexity, user flexibility and applicability compared to its solid counterpart. The electric field (E-field) at resonance at xoz cutting plane of the semi-spherical DRA without and with the lens for $\theta = 0°$ is shown in Fig. 7 (a) and (b). The E-field distinctly couples to the lens, exhibiting strong fields at the center and edges of the lens, resulting in a directorial effect that enhances the gain and directs the beam from the radiator. This is consistent with the fields observed when the lens is on the dipole in Fig. 2 (c). Fig. 7 (c) and (d) shows similar pattern when the lens is rotated to 30° and 45°, but some changes in the fields are observed as the lens is closer to the metallic ground plane.

Fig. 8 shows the S_{11} of the antennas at various angles. Both cases exhibit a stable matching when the lens moves. The simulated -10 dB frequency bands are 2.88 – 3.88 GHz (29.6%), 2.76 – 3.92 GHz (34.7%) for 1D and 2D beam steering antennas, respectively. Based on the theory illustrated in Section II, a good director effect of the lens was anticipated, which is consistent with the radiation patterns shown in Fig. 9. For simplicity, the beam steering performances are only shown at 3.2 GHz for 1D and 3.6 GHz for the 2D designs. A maximum

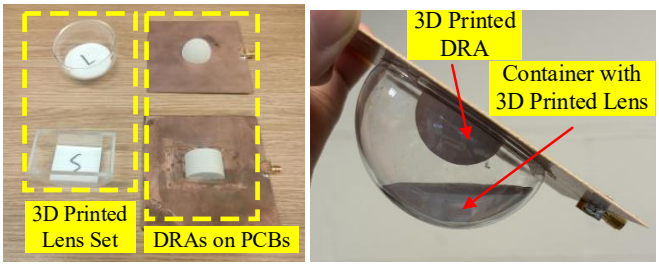

(a) (b)

Fig. 13. Solid based close-coupling guided lens development: (a) separate parts showing the 3D printed lenses and the DRAs, (b) 3D printed lens as part of 2D beam steering with semi-spherical DRA.

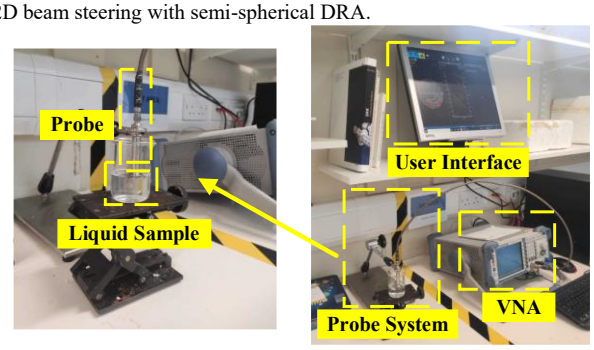

(a)

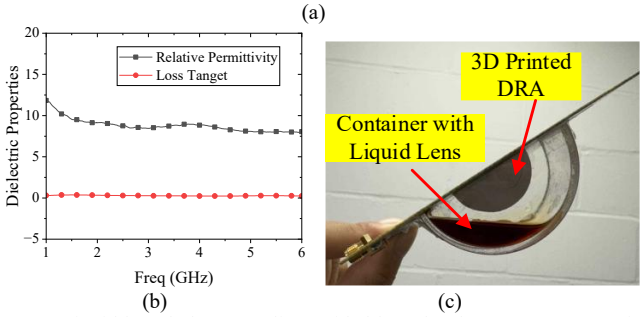

(b) (c)

Fig. 14. Liquid based close-coupling guided lens development: (a) setup for dielectric properties measurements of the liquid using SPEAG® DAK-3.5 probe system. (b) measured electrical properties of choline L-alanine (c) the ionic liquid as part of the 1D beam steering semi-cylindrical DRA.

beam steering angle of 30° and 35° are observed for 1D and 2D beam steering antennas, respectively when $\theta = 45°$. The gain is stable with less than 1.5 dB variation for the two cases. The 3 dB beamwidth is 54°, 54° and 88° for 1D, 2D x-scanning, 2D y-scanning beam steering cases, respectively, and the beam remains stable as the lenses rotate.

The effective beam steering bandwidth (3.2 – 3.7 GHz) is relatively narrower than that of -10-dB bandwidth, as shown in Fig. 9 (d). The side lobe level (SLL) or back lobe level is -16.8 dB for 1D beam steering, and -14.4 dB for 2D x-scanning and 2D y-scanning beam steering, which become lower with angle rotation.

C. Parametric Study

To have a better understanding of the lens effect, a parametric study about the properties of the lens was conducted. For simplicity, only the 2D semi-spherical DRA case is discussed, with the understanding that the 1D case would yield analogous results. Fig. 10 shows the simulated S_{11} and radiation patterns for different volume of material used for the lens, defined here by the height, D_{ls} in Fig. 4, where D_s is fixed at 7 mm. Too little or too much material deteriorates matching performance (Fig. 10 (a)). Too little material would also lead to insufficient director effect, thus reducing the gain and beam steering effect from the lens (Fig. 10 (b)). The gain enhancement, namely the director effect, is maximized when a specific volume of material is applied, corresponding to a height of 8 mm for D_{ls}. This volume of material provides good matching performance and robust director effect.

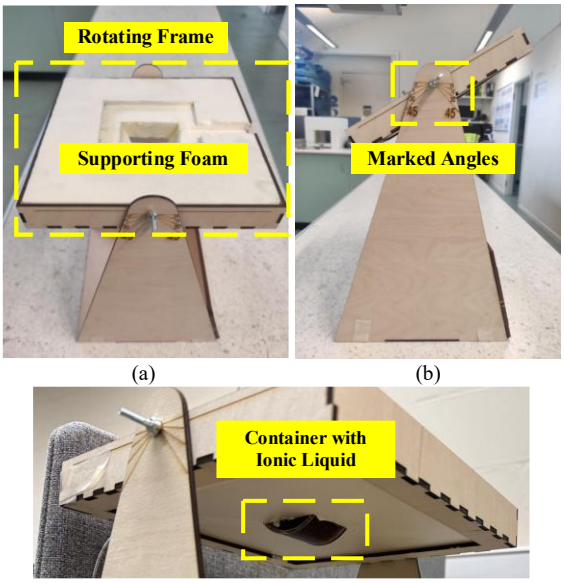

(a) (b)

(c)

Fig. 15. Fabricated frame that marks the rotation angles and holds the AUT to simulate practical scenarios of inclined aerial vehicles. (a) top view. (b) side view. (c) bottom view showing the container with liquid.

Fig. 11 and 12 present simulated results involving varying dielectric permittivity (ε_r) and loss tangent ($\tan\delta$). As ε_r decreases or $\tan\delta$ increases, the director effect diminishes, leading to a reduction in directed peak gain, and deteriorating matching performance. Taking into account both cost and performance considerations, the ionic liquid (reference) emerges as a compromise choice. Note that solid lenses can offer lower loss tangent, potentially enhancing S_{11} and gain.

III. Fabrication and Measurement

A. Fabrication

To fabricate the solid and liquid lenses, two separate procedures were used. The first involved utilizing 3D printed solid lenses that could move freely within a container. A set of solid lenses and DRAs were fabricated by 3D Printing as shown in Fig. 13 (a). The solid lenses and DRAs were fabricated using a Raise E2 3D printer with PREPERM® ABS1000 filament introduced in Section II. The DRAs were mounted on a printed circuit board (PCB) containing the ground plane with the coupling slot, feeding network, and SMA connector.

The semi-cylindrical (1D design) plastic container was created by laser cutting acrylic material, while the hemispherical one (2D design) was made of glass. The solid lenses were then manually inserted in the containers. Fig. 13 (b) displays a photo of the final 2D beam steering prototype with 3D printed lenses, demonstrating the guided lens behaviour after movement to about 45°.

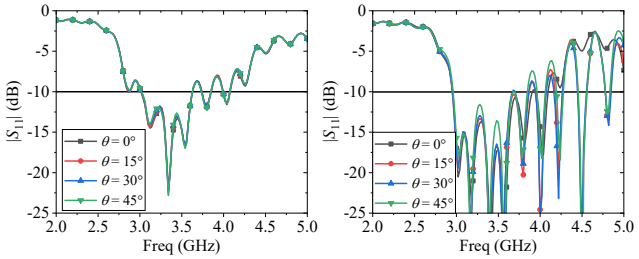

Fig. 16. Measured *S*-parameters for 1D beam steering semi-cylindrical DRA with (a) solid lens, (b) liquid lens.

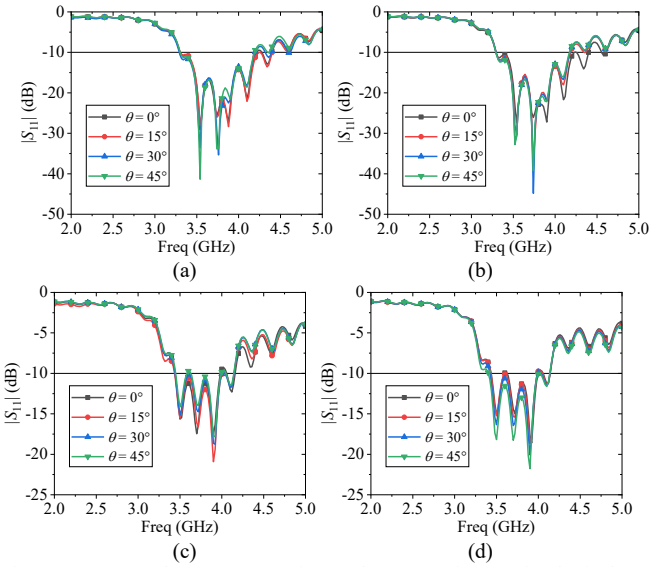

Fig. 17. Measured *S*-parameters for 2D beam steering semi-spherical DRA with (a) solid lens in x-scanning, (b) solid lens in y-scanning. (c) liquid lens in x-scanning, and (d) liquid lens in y-scanning.

The second method utilized liquid lenses, specifically made of choline L-alanine, synthesized by Iolitec Ionic Liquids Technologies GmbH. Such liquid is non-toxic and suitable for aerial vehicles and communication environments. The electrical properties of a synthesized ionic liquid choline L-alanine sample were measured using a SPEAG® DAK-3.5 probe system, covering a frequency range of 200 MHz to 20 GHz (Fig. 14 (a)). Distilled water was used for calibration to compensate for environmental temperature and humidity. Fig. 14 (b) presents the measured electrical properties. The dielectric permittivity decreases from over 10 at 1 GHz to about 9 between 2 GHz to 6 GHz, consistent with [27]. The measured loss tangent ranges from 0.2 to 0.3 between 2 GHz and 6 GHz, slightly higher than the expected value (0.1) in simulations. Nonetheless, it is worth noting that the loss tangent mainly impacts the maximum gain based on the parametric study analysis given in Fig. (12), and this minor difference should not significantly affect the performance of the lens. After confirming the dielectric properties of the liquid, it was placed with the DRAs on corresponding containers for testing, as shown in Fig. 14 (c) for the 1D configuration.

While liquid lenses offer flexibility, their higher loss tangents may limit their use in high-precision applications. Conversely, solid lenses provide enhanced gain stability at the expense of adaptability. For verification, four sets of antennas were fabricated in total for subsequent measurements: 1D and 2D

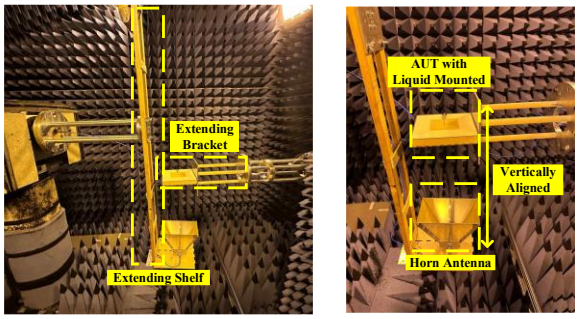

Fig. 18. Transformed chamber setup for the far field measurement.

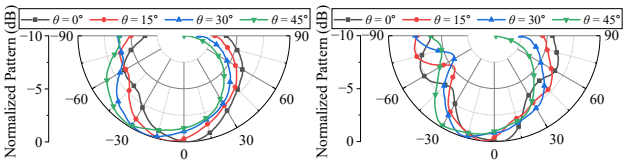

Fig. 19. Measured radiation pattern for 1D beam steering semi-cylindrical DRA with (a) solid lens, and (b) liquid lens at 3.2 GHz.

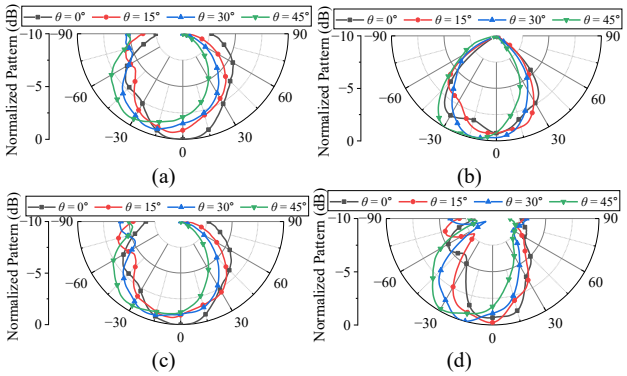

Fig. 20. Measured radiation pattern for 2D beam steering semi-spherical DRA at 3.6 GHz with (a) solid lens in x-scanning, (b) solid lens in y-scanning, (c) liquid lens in x-scanning, and (d) liquid lens in y-scanning.

configurations with solid lenses, and 1D and 2D configurations with liquid lenses.

B. Measurements

A measurement setup was designed to simulate the practical scenarios in aerial vehicles and communication systems, where specific inclined angles on the mounting structures are taken into account. To ensure precise control of the structure's rotation, a frame with angle markings was constructed, as shown in Fig. 15. During S_{11} measurements, the entire structure was manually rotated to align with these markings, allowing for precise angle adjustments. Additionally, a polystyrene foam support was crafted using a Computer Numerical Controlled (CNC) cutting machine to secure the Antenna Under Test (AUT).

The measured S_{11} is presented in Fig. 16 and 17. There is consistency on S_{11} between the solid and liquid lenses. However, a slight deterioration and a frequency shift to higher frequency bands are observed for both 1D and 2D beam steering DRAs. This could be attributed to infilled air and fabrication errors during the 3D-printing process, which may reduce the DRAs' equivalent permittivity and consequently shift the resonant frequency. Nevertheless, the measured

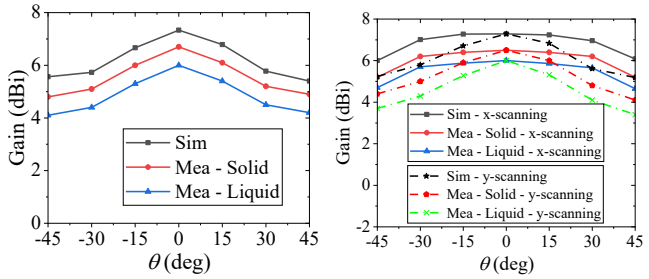

Fig. 21. Simulated and measured gain at broadside direction when rotating. (a) 1D beam steering DRA at 3.2 GHz. (b) 2D beam steering DRA with x/ y-scanning at 3.6 GHz.

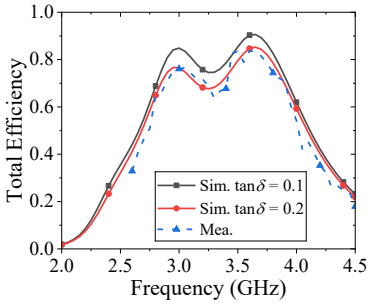

Fig. 22. Efficiency of the 1D beam steering semi-cylindrical DRA with liquid lens at $\theta = 45°$.

frequency bands of 2.95 – 4.09 GHz (32.5%) for 1D and 3.12 – 4.12 GHz (27.6%) for 2D beam steering antennas with liquid lenses still aligns with simulated results.

After verifying the S_{11} operation of the lens antennas across the desired frequency range, far-field measurements were conducted in an anechoic chamber to evaluate the beam steering behaviour of the close-coupling guided lenses. To enable far-field measurement, an extending shelf, with a vertically positioned horn antenna at the bottom, was constructed on the transmitter side, while an extending bracket was attached on the receiver side to secure the AUT with the loaded liquid as shown in Fig. 18. This configuration enabled vertical alignment of the transmitter and receiver antennas, facilitating the acquisition of the far-field radiation pattern by rotating the extension shelf along with the mounted horn antenna. The precise alignment and horizontal orientation of the AUT were ensured using steel plumb bobs and spirit levels. Different inclined angles were measured in this setup to replicate practical scenarios of aerial vehicles and communication systems involving tilts.

Fig. 19 and 20 show the measured radiation patterns, revealing consistency on radiation patterns between the solid and liquid lenses. For all of the 1D, 2D x-scanning and 2D y-scanning beam steering cases, a maximum 35° beam steering angle is achieved when the liquid reaches its maximum rotation angle of $\theta = 45°$, and less than 1.5 dB gain variation. In some figures, the SLL appears degraded, such as -5 dB in liquid lens y-scanning case (Fig. 20 (d)). This could be attributed to fabrication and measurement errors. However, it is evident that, in most cases, only one main beam is observed. The beam steering bandwidth is slightly narrower than the -10 dB bandwidth, which aligns with simulation results. The radiation pattern varies within the frequency bands, but the overall tendency remains consistent.

TABLE II
COMPARISON BETWEEN THE PROPOSED IDEA AND OTHER COUNTERPARTS

Ref.	[12]	[20]	[21]	This work
Antenna Type	Patch + dipole	Mechanical weight rotation	DRA + ball lens	Guided lens + any radiator (e.g. dipole or DRA)
Beam steering	1D	1D	2D	1D or 2D
AC Power	Need	No	No	No
Add-on to existing aerial devices	No	No	Limited	Yes
Lens Type	N. A.	N. A.	Only solid	Solid/ liquid
Volume of main part	N. A.	Reflector: 23.6 cm^3	Ball lens: 33.51 cm^3	1D lens: 6.7 cm^3 2D lens: 5.5 cm^3
Scanning Angle	±35°	±360°	±40°	DRA: ±35° Dipole: ±360°
Peak Gain	6.9 dBi	6.8 dBi	7.9 dBi	DRA: 7.5 dBi Dipole: 5.2 dBi

Fig. 21 presents the measured broadside gain during lens rotation. Compared with the results for the solid lenses, the liquid lenses exhibit a larger gain loss, likely due to the larger loss tangent and lower permittivity, as discussed in Part A. However, the measured results still demonstrate less than 1.5 dB loss in all cases compared to simulated results, indicating good agreement between the two. The simulated and measured radiation efficiencies for the 1D beam-steering semi-cylindrical DRA with a liquid lens at rotation angle $\theta = 45°$ are presented in Fig. 22. This angle was selected as a representative case, as other steering angles follow a similar trend. The measured efficiency is consistently lower than the simulated one, which can be primarily attributed to the higher loss tangent of the ionic liquid, as previously characterized in Fig. 14. By updating the simulated model to reflect a more realistic loss tangent value (from 0.1 to 0.2), a close agreement between the modified simulation and the measured efficiency was achieved. This observation is consistent with the gain reduction seen in Fig. 21. As indicated in the parametric study, the increased dielectric loss mainly affects the realized gain, while its influence on beam-steering behavior remains minimal.

While higher-gain antennas are typically advantageous for long-range communications, they often require larger physical dimensions, which may not be suitable for compact UAV platforms. An antenna gain in the range of 0 – 8 dBi is more appropriate for short-range (< 5 km) civil UAV applications, such as telemetry, remote control [28], and First Person View (FPV) systems [29], where low weight and size are critical design constraints. The gain could be further enhanced by applying other auxiliary parts, such as stacked DRA [30], patch/dielectric hybrid structure [31], or metasurface [32]. These methods are efficient in enhancing the gain without increasing the dimensions, profile or changing the radiated beam characteristics.

IV. DISCUSSION

A comparison between the proposed idea with previously reported counterparts is illustrated in Table II. Only the

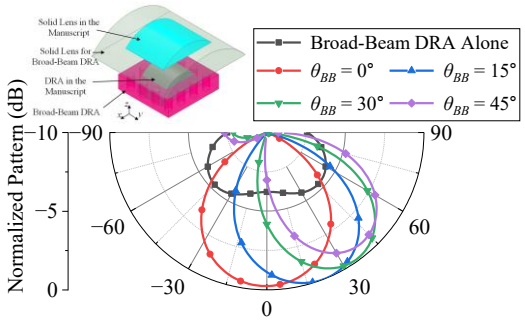

Fig. 23. Gain enhancement and normalized radiation patterns of the broad-beam DRA with and without the solid lens. Here, θ_{BB} denotes the rotation angle of the lens for the broad-beam DRA.

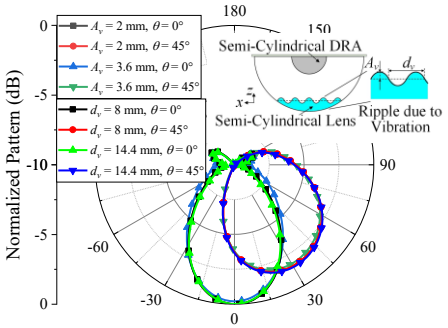

Fig. 24. Simulated matching and radiation performance of the proposed design with uneven lens surface.

relevant works suitable for down-facing beam steering for aerial vehicles and communication applications are listed. Compared with conventional reconfigurable antennas counterparts for aerial applications [9-16], the proposed concept eliminates the need for additional controlling system and A.C. power, significantly reducing complexity. Unlike the rotatable Yagi antenna [20], which achieves beam steering in only one direction and the balls lens that is limited to 2D, the proposed idea can be applied to 1D and 2D beam steering. Besides, this work employs a close-coupling guided lens as an add-on to enhance gain and steer the beam of the primary radiator. This is as significant advantage compared to previous work as it can be integrated with most antennas and aerial devices as part of their enclosure. The ball lens in [21] could not be applied directly to existing aerial devices as it uses a cord which limits movement. Even more problematic would be the use of [20] with a fixed ground plane, reflector and director. Furthermore, the proposed approach utilizes a container for the lenses, enhancing mechanical robustness and allowing not only solid but also liquid materials to be used as lenses. Furthermore, only a minimal volume for the lens (< 7 cm^3 equivalent volume) is required, distinguishing it from prior design that requires a large spherical ball (~ 34 cm^3). This could lead to cost reduction and enhanced practicality. Similarly to [20], the proposed 1D design achieves 360° beam steering in one direction and enhanced side stability in the other direction when using the solid lens, which cannot be achieve with [21]. The proposed 2D design utilizing a DRA achieved scanning within ±35° in all directions. Nevertheless, its add-on nature suggests the potential for achieving even wider angles, enabling full 3D 360° scanning when implemented with different antenna structures. The peak gain enhancement is comparable for all the techniques. All of this makes the proposed close-coupling guided lens technology highly suitable for deployment as a powerless add-on solution for aerial vehicles and communication systems in scenarios involving inclines.

Loading a close-coupling lens onto an antenna with an isotropic or broad radiation pattern can potentially yield more consistent directivity in the gravitational direction. To verify this, a solid lens was applied to a broad-beam DRA with a 3-dB beamwidth of 223°, and the corresponding results are presented in Fig. 23 [33]. A gain enhancement of 6 dB and a beam steering angle of 40° were achieved with a lens rotation angle of θ_{BB} = 45°, both indicating improved directivity consistency. However, this improvement comes at the cost of a significantly increased antenna and lens volume.

A simulation was conducted to model the uneven surface of the liquid lens caused by vibration in practical UAV scenarios. The perturbation was represented as ripples with amplitude A_v and spacing d_v along the rotation direction. As shown in Fig. 24, the impact of surface irregularities on beam steering performance is limited, with gain degradation remaining below 0.25 dB. These results demonstrate the robustness of the proposed beam steering structure.

V. Conclusion

In this paper, the concept of gravity triggered pattern-reconfigurable antenna based on close-coupling guided lenses has been demonstrated. By loading lenses onto predesigned curved containers, the gain can be enhanced, and beam steering can be achieved. When the lens moves to a certain angle by the effect of gravity, the main beam of the radiator can be directed to the direction where the lens is positioned. Complete 360° beam steering can be realized when the lens is applied to a cylindrical container with a dipole antenna. In more application-based scenarios using DRAs with cylindrical and semi-spherical containers, both 1D and full half-space (2D) beam steering can be realized. Both liquid and solid lenses having exactly the same dimensions and electrical characteristics can be used. A maximum ±35° beam steering angle has been achieved when combined with the DRAs, with less than 1.5 dB variation when maximum rotation angle θ = ±45°. The consistency between simulated and measured results, as well as between solid and liquid lenses, confirmed the feasibility of the concept. It is noteworthy that the antenna's beam scanning angle has been intentionally limited ±45° rotation angle of the lens due to concerns related to lens deformation and associated uncertainties.

The proposed concept stands out from conventional electrically controlled beam steering systems and previously gravity-based designs. It offers the advantages of being an add-on solution for most antennas, flexibility of using solid or liquid lenses, reduced material usage and higher beam steering angle and configuration possibilities (360º, 1D, 2D).

The main application is in antennas integrated into platforms requiring static or dynamic tilts. In dynamic tilts, such as those on aerial vehicles like aircraft, UAVs, high altitude balloons, changes in acceleration and turbulences may impact the performance of the proposed system. Solid or semisolid lenses that respond more slowly to sudden movements could be

utilized in such scenarios. Future assessment of the communication system could be realized by developing a simplified testbed that simulates UAV angular dynamics, enabling real-time evaluation of communication metrics such as link quality and beam tracking stability. Future research could also explore broader applications, such as disaster recovery networks and low-cost beam steering solutions for maritime or satellite systems. Investigating the use of advanced materials and hybrid mechanical-electrical steering mechanisms may further enhance the concept's adaptability and robustness in dynamic environments.

ACKNOWLEDGEMENT

The authors would like to thank Dr. Viktorija Makarovaite, Antonio Mendoza, Keith Greenhow, Joseph Hill, Cheryl Banton and KEYENCE UK LTD for their support. This work was funded by the EPSRC grant EP/S005625/1, and Royal Society - International Exchanges 2019 Cost Share (NSFC) (Ref: IEC\NSFC\191780).

REFERENCES

[1] Y.-X. Sun, D. Wu, X. S. Fang, and J. Ren, "On-Glass Grid Structure and Its Application in Highly-Transparent Antenna for Internet of Vehicles," *IEEE Transactions on Vehicular Technology,* vol. 72, no. 1, pp. 93-101, 2023-01-01 2023, doi: 10.1109/tvt.2022.3205899.

[2] J. Zhang, H. Zhong, J. Cui, M. Tian, Y. Xu, and L. Liu, "Edge Computing-Based Privacy-Preserving Authentication Framework and Protocol for 5G-Enabled Vehicular Networks," *IEEE Transactions on Vehicular Technology,* vol. 69, no. 7, pp. 7940-7954, 2020-07-01 2020, doi: 10.1109/tvt.2020.2994144.

[3] X. Ge, H. Cheng, G. Mao, Y. Yang, and S. Tu, "Vehicular Communications for 5G Cooperative Small-Cell Networks," *IEEE Transactions on Vehicular Technology,* vol. 65, no. 10, pp. 7882-7894, 2016-10-01 2016, doi: 10.1109/tvt.2016.2539285.

[4] J. Wang, C. Jiang, Z. Han, Y. Ren, and L. Hanzo, "Internet of Vehicles: Sensing-Aided Transportation Information Collection and Diffusion," *IEEE Transactions on Vehicular Technology,* vol. 67, no. 5, pp. 3813-3825, 2018-05-01 2018, doi: 10.1109/tvt.2018.2796443.

[5] Q. Kong, R. Lu, F. Yin, and S. Cui, "Blockchain-Based Privacy-Preserving Driver Monitoring for MaaS in the Vehicular IoT," *IEEE Transactions on Vehicular Technology,* vol. 70, no. 4, pp. 3788-3799, 2021-04-01 2021, doi: 10.1109/tvt.2021.3064834.

[6] Q. F. Zhou, A. Huang, M. Peng, F. Qu, and L. Fan, "On the Mode Switching of Reconfigurable-Antenna-Based Blind Interference Alignment," *IEEE Transactions on Vehicular Technology,* vol. 66, no. 8, pp. 6958-6968, 2017-08-01 2017, doi: 10.1109/tvt.2017.2663200.

[7] B. Moision *et al.*, *Demonstration of free-space optical communication for long-range data links between balloons on Project Loon* (SPIE LASE). SPIE, 2017.

[8] M. D. N. Anjum, H. Wang, and H. Fang, "Percolation analysis of large-scale wireless balloon networks," *Digital Communications and Networks,* vol. 5, no. 2, pp. 84-93, 2019/05/01/ 2019, doi: https://doi.org/10.1016/j.dcan.2018.03.001.

[9] S. Gaya, A. Hamza, O. Sokunbi, S. I. M. Sheikh, and H. Attia, "Electronically Switchable Frequency and Pattern Reconfigurable Segmented Patch Antenna for Internet of Vehicles," *IEEE Internet of Things Journal,* vol. 11, no. 10, pp. 17840-17851, 2024-05-15 2024, doi: 10.1109/jiot.2024.3362906.

[10] B. Feng, H. Li, L. Rao, X. Ding, C.-Y.-D. Sim, and K. L. Chung, "An Aperture-Shared Vehicular Antenna With Large Frequency Ratio and Pattern Diversity for Future 5G Millimeter-Wave and DSRC Applications," *IEEE Transactions on Vehicular Technology,* vol. 73, no. 2, pp. 1942-1956, 2024-02-01 2024, doi: 10.1109/tvt.2023.3320170.

[11] D. Piazza, P. Mookiah, M. D'Amico, and K. R. Dandekar, "Experimental Analysis of Pattern and Polarization Reconfigurable Circular Patch Antennas for MIMO Systems," *IEEE Transactions on Vehicular Technology,* vol. 59, no. 5, pp. 2352-2362, 2010-01-01 2010, doi: 10.1109/tvt.2010.2043275.

[12] Z. Wang, S. Liu, and Y. Dong, "Compact Wideband Pattern Reconfigurable Antennas Inspired by End-Fire Structure for 5G Vehicular Communication," *IEEE Transactions on Vehicular Technology,* vol. 71, no. 5, pp. 4655-4664, 2022-05-01 2022, doi: 10.1109/tvt.2022.3152354.

[13] L. Marantis, D. Rongas, A. Paraskevopoulos, C. Oikonomopoulos - Zachos, and A. Kanatas, "Pattern reconfigurable ESPAR antenna for vehicle - to - vehicle communications," *IET Microwaves, Antennas & Propagation,* vol. 12, no. 3, pp. 280-286, 2018-02-01 2018, doi: 10.1049/iet-map.2017.0209.

[14] B. Ashvanth, B. Partibane, M. G. N. Alsath, and R. Kalidoss, "Gain enhanced multipattern reconfigurable antenna for vehicular communications," *International Journal of RF and Microwave Computer-Aided Engineering,* vol. 30, no. 6, 2020-06-01 2020, doi: 10.1002/mmce.22192.

[15] B. Ashvanth, B. Partibane, M. G. Nabi Alsath, and R. Kalidoss, "Tunable dual band antenna with multipattern reconfiguration for vehicular applications," *International Journal of RF and Microwave Computer-Aided Engineering,* vol. 29, no. 12, 2019-12-01 2019, doi: 10.1002/mmce.21973.

[16] F. Gao and H. Sun, "A Radiation-Pattern Reconfigurable Antenna Array for Vehicular Communications," *Sensors,* vol. 24, no. 13, p. 4136, 2024-06-26 2024, doi: 10.3390/s24134136.

[17] J. Yang, J. Li, S. Zhou, D. Li, and G. Yang, "A Polarization and Frequency Reconfigurable Microstrip Antenna for Vehicular Communication System Application," *IEEE Transactions on Vehicular Technology,* vol. 72, no. 1, pp. 623-631, 2023-01-01 2023, doi: 10.1109/tvt.2022.3202973.

[18] G. Kahmen and H. Schumacher, "Interactive Design of MEMS Varactors With High Accuracy and Application in an Ultralow Noise MEMS-Based RF VCO," *IEEE Transactions on Microwave Theory and Techniques,* vol. 65, no. 10, pp. 3578-3584, 2017-10-01 2017, doi: 10.1109/tmtt.2017.2742482.

[19] I. J. Gupta, I. M. Weiss, and A. W. Morrison, "Desired Features of Adaptive Antenna Arrays for GNSS Receivers," *Proceedings of the IEEE,* vol. 104, no. 6, pp. 1195-1206, 2016-06-01 2016, doi: 10.1109/jproc.2016.2524416.

[20] L. Li, A. Fu, H. Xiong, J. Han, and W. Wu, "Coaxial Line and Ground Separated Beam-Steering Yagi–Uda Antenna Controlled by Gravity," *IEEE Antennas and Wireless Propagation Letters,* vol. 22, no. 9, pp. 2100-2104, 2023-09-01 2023, doi: 10.1109/lawp.2023.3276006.

[21] Z. Chen, Q. Liu, B. Sanz-Izquierdo, H. Liu, J. Yu, and X. Chen, "A Wideband Circular-Polarized Beam Steering Dielectric Resonator Antenna Using Gravitational Ball Lens," *IEEE Transactions on Antennas and Propagation,* vol. 69, no. 5, pp. 2963-2968, 2021, doi: 10.1109/TAP.2020.3025243.

[22] C. Song *et al.*, "Passive Beam-Steering Gravitational Liquid Antennas," *IEEE Transactions on Antennas and Propagation,* vol. 68, no. 4, pp. 3207-3212, 2020-04-01 2020, doi: 10.1109/tap.2019.2937362.

[23] X. Yan, L. Li, H. C. Zhang, and J. Y. Han, "Broadband Polarization-Reconfigurable Liquid Dielectric Resonator Antenna Controlled by Gravity," *IEEE Antennas and Wireless Propagation Letters,* vol. 21, no. 10, pp. 2105-2109, 2022-10-01 2022, doi: 10.1109/lawp.2022.3191314.

[24] F. Sun, L. Xing, Q. Xu, X. Kong, H. Wang, and G. Zhang, "An Attitude-Independent Liquid Dielectric Resonant Antenna," *IEEE Antennas and Wireless Propagation Letters,* vol. 21, no. 1, pp. 154-157, 2022-01-01 2022, doi: 10.1109/lawp.2021.3121772.

[25] J. L. Volakis, R. C. Johnson, and H. Jasik, *Antenna engineering handbook*. 2007.

[26] F. Ahmed, T. Hayat, M. U. Afzal, S. Zhang, K. P. Esselle, and W. G. Whittow, "3-D Printable Synthetic Metasurface to Realize 2-D Beam-Steering Antenna," *IEEE Open Journal of Antennas and Propagation,* vol. 4, pp. 506-519, 2023-01-01 2023, doi: 10.1109/ojap.2023.3274782.

[27] C. Song, E. L. Bennett, J. Xiao, A. Alieldin, K.-M. Luk, and Y. Huang, "Metasurfaced, broadband, and circularly polarized liquid antennas using a simple structure," *IEEE Transactions on Antennas Propagation,* vol. 67, no. 7, pp. 4907-4913, 2019.

[28] J.-M. Fernandez Gonzalez, P. Padilla, J. F. Valenzuela-Valdes, J.-L. Padilla, and M. Sierra-Perez, "An Embedded Lightweight Folded Printed Quadrifilar Helix Antenna: UAV telemetry and remote control systems," *IEEE Antennas and Propagation Magazine,* vol. 59, no. 3, pp. 69-76, 2017-06-01 2017, doi: 10.1109/map.2017.2686702.

[29] S. Kim and J. Choi, "Beam steering antenna with reconfigurable parasitic elements for FPV drone applications," *Microwave and Optical Technology Letters,* vol. 60, no. 9, pp. 2173-2177, 2018-09-01 2018, doi: 10.1002/mop.31320.

[30] Y. M. Pan and S. Y. Zheng, "A Low-Profile Stacked Dielectric Resonator Antenna With High-Gain and Wide Bandwidth," *IEEE Antennas and Wireless Propagation Letters,* vol. 15, pp. 68-71, 2016-01-01 2016, doi: 10.1109/lawp.2015.2429686.

[31] A. Perron, T. A. Denidni, and A.-R. Sebak, "High-Gain Hybrid Dielectric Resonator Antenna for Millimeter-Wave Applications: Design and Implementation," *IEEE Transactions on Antennas and Propagation,* vol. 57, no. 10, pp. 2882-2892, 2009-10-01 2009, doi: 10.1109/tap.2009.2029292.

[32] M. A. J. Al-Hasan, T. A. Denidni, and A. R. Sebak, "Millimeter-Wave EBG-Based Aperture-Coupled Dielectric Resonator Antenna," *IEEE Transactions on Antennas and Propagation,* vol. 61, no. 8, pp. 4354-4357, 2013-08-01 2013, doi: 10.1109/tap.2013.2262667.

[33] Z.-K. Chen, L. Zhang, Z. Weng, and R.-Y. Li, "Wideband Wide-Beam Hybrid Dielectric Resonator Antenna Using Uniaxial Material," *IEEE Antennas and Wireless Propagation Letters,* vol. 22, no. 1, pp. 124-128, 2023-01-01 2023, doi: 10.1109/lawp.2022.3204552.